J Nanopart Res (2023) 25:258
https://doi.org/10.1007/s11051-023-05902-3

RESEARCH PAPER

Evaluation of the toxicity of ZnO nanoparticles obtained by a chemical route on the nasal respiratory epithelium of the biomodel *Mus musculus*

K. E. Mosquera-Murillo · A. M. Castañeda-Manquillo · K. L. Ángel-Camilo · P. A. Arciniegas-Grijalba · M. M. Ramírez de Valdenebro · L. P. Mosquera-Sanchez · I. A. Meza-Cabrera · J. E. Rodriguez-Paez

Received: 14 August 2023 / Accepted: 23 November 2023 / Published online: 15 December 2023

Abstract Zinc oxide nanoparticles (ZnO-NPs) have antimicrobial and a number of other properties, rendering apt their use in biomedicine, environmental remediation, agriculture, and other fields. Given the potential use of these nanoparticles (NPs) in these areas, it is necessary to determine their toxic effects on biological systems. This work therefore analyzed the histological changes in the respiratory nasal epithelium of *Mus musculus* biomodels exposed to atmospheres containing ZnO-NPs at different concentrations (6, 15, and 40 mg/m^3). The NPs were synthesized using the Pechini polymeric complex method and characterized using techniques such as IR and Raman spectroscopies, X-ray diffraction (XRD), transmission (TEM), and scanning electron microscopy (SEM). The ZnO-NPs obtained had a wurtzite-type structure, with spheroidal morphology and a particle size of ~ 50 nm, and the Raman spectrum showed the presence of defects in its structure. The results of the treatments to which the biomodels were subjected showed that the inhalation of ZnO-NPs caused significant morphological changes in their nasal epithelium (squamous metaplasia and vascular congestion) and an acute inflammatory response when exposed to high concentrations of NPs (40 and 15 mg/m^3).

Keywords ZnO nanoparticles · Chemical synthesis · Characterization · Toxicity · Nasal respiratory epithelium · *Mus musculus*

Introduction

The field of nanotechnology is one of enormous current interest, involving a wide range of disciplines and potential applications [1, 2]. Specifically, considering

K. E. Mosquera-Murillo · P. A. Arciniegas-Grijalba · M. M. R. de Valdenebro · L. P. Mosquera-Sanchez
Faculty of Exact Natural Sciences and Education, Microscopy and Image Analysis Research Group (GIMAI), Universidad del Cauca, Popayán, Colombia

A. M. Castañeda-Manquillo · J. E. Rodriguez-Paez (✉)
Faculty of Exact Natural Sciences and Education, Research Group On Science and Technology of Ceramic Materials (CYTEMAC), Department of Physics, Universidad del Cauca, Popayán, Colombia
e-mail: jnpaez@unicauca.edu.co

K. L. Ángel-Camilo
Faculty of Exact Natural Sciences and Education
Herpetological and Toxicological Research Group, Department of Biology, Universidad del Cauca, Popayán, Colombia

K. L. Ángel-Camilo
Faculty of Pharmacy, Dentistry and Nursing, Post-Graduation Program in Pharmaceutical Sciences, Universidade Federal Do Ceará, Fortaleza, Brazil

I. A. Meza-Cabrera
Faculty of Health Sciences, Department of Pathology, Universidad del Cauca, Popayán, Colombia

the world population and its projected increase (by 2050 it is considered a figure of 9700 million people will be reached), it is necessary to improve food production. The use of nanotechnology — specifically the use of nanoparticles (NPs) — is currently thus being researched and assessed in order to improve and increase the efficiency of agricultural crops [3–5]; the capacity of NPs as a fertilizer [6], fungicide and insecticide [7], as well as in pest and disease control in various crops, including coffee[8–10], tomato [11], wheat [12], and avocado [13], etc. Other research has considered the strengthening of crop productivity at low costs [14].

Another field of great interest for the use of NPs is biomedicine, where research has been carried out related to the potential use of nanomaterials as vehicles for targeted drug delivery, avoiding adverse or secondary effects, and in the production of drugs for the treatment of neurodegenerative diseases (Parkinson, Alzheimer, etc.) [15], cardiovascular and autoimmune diseases (cancer, HIV, etc.) [16], etc. In addition, the use of NPs in gene administration, separation and purification of molecules in biological cells, detection of pathogens and proteins, tissue engineering, medical imaging, among other potential applications has been assessed [17–19].

Zinc oxide nanoparticles (ZnO-NPs) constitute one of the nanomaterials of current scientific, economic, and industrial interest due to their unique optical, electrical, thermal, and photocatalytic properties [20, 21]. These properties have allowed their use in the manufacture of cosmetics and textiles [22], as well as in nanophotonics, nanoelectronics, and nano-biotechnology, among other applications[20, 21, 23–25]. In addition, their antimicrobial and anticancer activity has led to consideration of their use in biomedicine, environmental remediation, and agriculture [17, 26]. Zinc oxide (ZnO) is an inorganic, non-toxic compound that can have, mainly, three types of crystalline structures: wurtzite, zinc blende, and rock salt [20, 21, 23], wurtzite being the most thermodynamically stable crystalline phase (*P63mc* space group). ZnO is a broadband semiconductor, with a band gap of ~ 3.3 eV at room temperature. To obtain ZnO-NPs with specific physicochemical characteristics, in a controlled and reproducible way, different processes have been used, with the following methods to the fore: sol–gel, polymeric complex (Pechini), solvothermal and hydrothermal, controlled precipitation, and green chemistry [27, 28]. In particular, in this work, the Pechini method was used [29–31].

Given the great application potential of nanoparticles in various fields due to their unique properties, specifically ZnO-NPs, it is necessary to evaluate their toxicity to ensure that they do not cause negative effects on human health, the environment and, in general, to biological systems [32–34]. This knowledge will allow standardizing appropriate use of nanotechnology, certifying a reliable and safe use of nanoparticles [33–35]. A branch of toxicology is thus dedicated to assessing the toxicity (harmful impacts) of nanomaterials and this has been called nanotoxicology [36, 37]. This area of knowledge therefore studies the interactions of NPs with living organisms, especially to determine how functioning at the molecular and cellular level might be affected [38, 39]. Nanotoxicology has shown that, given the small size of NPs, they are very reactive, both biologically and chemically, which influences their toxicity. Being of nanometric size would allow them to enter cells and various organelles, effectively crossing tissues and cell membranes, for example, generating oxygen species (ROS) and free radicals, which can cause mitochondrial damage, lysosomal dysfunction, and ultimately, mutation, and cell death [32]. Previous works have reported alterations in living systems, such as interstitial inflammation and lung toxicity, endoplasmic reticulum stress, liver toxicity, and central nervous system toxicity induced by carbon, silver, gold, and titanium dioxide NPs, respectively [39]. Also, alterations in iron homeostasis, cytotoxic activity, and oxidative stress have been found in the heart, brain, liver, and lungs, due to the action of iron oxide NPs and those of a ceramic nature, respectively. Additionally, exposure to silica NPs has led to platelet aggregation, reproductive, and physiological toxicity, and in the presence of titanium dioxide NPs, alterations in the exocytosis process in serotonin mast cells were observed [39]. In addition, these studies have made it possible to determine the effect of the physicochemical characteristics of the NPs, defined by the synthesis route used to obtain them, on their bioactivity [40].

To assess the toxic effects of the NPs, the biomodels are exposed to them by dermatological, oral, and inhalation routes, the latter being that used in this work. Of the biomodels used, various species of fish, amphibians, and mammals have been used and, within the latter, the

most widely used are laboratory rodents, since they have anatomical, histological, and physiological characteristics that coincide with those of humans. In addition, the exposure times to the NPs depend on the average life of the biomodel, highlighting the acute studies, short-term exposures (days or up to a week), and the chronic ones, prolonged exposure (months, years or sometimes and can last all their life) [41].

In the specific case of ZnO-NPs, their toxicity has been evaluated in several biomodels and it has been found that the administration of ZnO-NPs, in the ingestion of female rats, for example, caused changes in the blood analysis and pathological lesions in tissues of the stomach, liver, and kidney [42]. Moreover, in males, it produced negative effects on liver function, generating histological alterations in the liver, cytochrome enzymes, liver enzymes, and oxidative stress [43]. In the work of Wang et al. [44], the researchers found that the ingestion of ZnO-NPs in male mice caused loss of body weight, an increase in Zn content in the blood and the mRNA expression of genes related to the metabolism of zinc. Specifically, after inhalation of NPs, the results indicated that they entered the body and could move to other parts of the body and induce effects such as: allergic and eosinophilic inflammation in the respiratory tract [45, 46], and alterations in various organs such as the liver, kidney, lung, spleen, brain, pancreas, blood, etc. [45, 47–49], mainly. Furthermore, other studies indicate that these NPs could cause minimal lung inflammation, cytotoxicity, or significant changes at the organism level [50].

Considering the above, in this work, ZnO-NPs were obtained using a chemical route (Pechini method) and the toxic effect produced by their inhalation on the nasal respiratory epithelium (NRE) of the biomodel *Mus musculus* was assessed. The NRE was chosen as the object of study because it is located in the nasal cavity and is in direct contact with the substances that enter via this route [51]. In addition, the NRE contains hair cells that act as "mucociliary sweepers," constituting a defense mechanism or barrier against pathogens or small particles that try to enter the body. It is thus considered the first defense of the respiratory system [52]. The results obtained in this work can therefore be considered novel because they provide information about the first contact of the ZnO-NPs with the respiratory system when inhaled, both by humans and animals, in applications that involve their spraying, for example, in agriculture as a nanofungicide, nanopesticide, and/or nanofertilizer.

Materials and methods

Synthesis of ZnO-NPs

The ZnO-NPs were obtained by chemical route using the Pechini method [31, 53, 54]. For this, zinc acetate dihydrate ($Zn(CH_3COO)_2$-$2H_2O$ – Merck) was used as a precursor of the cation of interest, specifically 2.70 g of the reagent, and to promote the polyesterification reaction, which characterizes this synthesis method, 2.60 g of citric acid ($C_6H_8O_7$-H_2O—Merck) and 3.10 g of ethylene glycol ($C_2H_6O_2$—Merck) were used. Initially, the ethylene glycol was heated to 70 ºC, to which citric acid was slowly added. Simultaneously, in another beaker, the zinc precursor was diluted in 13.5 g of distilled water. Both solutions were kept under continuous stirring until a homogeneous solution was obtained. The two solutions were then mixed, at room temperature and with constant stirring, until a mixture with a translucent appearance was obtained. Next, ammonium hydroxide (NH_4OH-Merck) was added in a controlled manner to the resulting mixture, until reaching a pH of 9 (working pH), to favor the development of hydrolysis and condensation reactions in the system. During the addition of NH_4OH, the added volume of the weak base, the pH value, and the temperature of the system were recorded, in order to obtain a potentiometric titration curve, which allowed controlling the process and ensuring its reproducibility.

The mixture obtained was heated at 130 ºC for 6 h with continuous stirring, until a whitish resin was formed. This resin was then subjected to a heat treatment of 300 °C, in a kitchen oven (Haceb brand) for 5 h, obtaining a precalcined brown color, which was macerated in an agate mortar. Finally, the precalcined material was subjected to a heat treatment at 550 °C using a muffle (Terrigeno), which was programmed at a heating rate of 5 °C/min. A diagram of the process used to obtain the ZnO of interest is shown in Fig. 1.

Characterization of the synthesized ZnO

The obtained ZnO ceramic powder was characterized using conventional analysis techniques. To identify

the functional groups, present in the solid, Fourier Transform Infrared (FT-IR) spectroscopy was used. The samples to be analyzed were mixed with potassium bromide (KBr), in a concentration of 10% to 90% (p/p) respectively. This mixture was subjected to pressure, using a stainless-steel die, until it formed a translucent pellet that was placed in the sample holder of the spectrophotometer (Thermo Nicolet IR 200) with Ezominic 32 software, for their respective analysis. The number of sweeps being 32, with a resolution of 16 cm^{-1}/s, and the sweep was performed between 400 and 4000 cm^{-1}.

X-ray diffraction (XRD) was used to determine the amorphous or crystalline nature of the synthesized material and the crystalline phases present. For this, a Bruker model D8 Advance unit with DaVinci Geometry was used. Data were recorded in the range of 2° and 70°, in 2θ, with a step: 0.02035° (2θ) and time per step of 0.6 s.

The agglomeration state of the synthesized ZnO powder, as well as its morphology and particle size, was determined using electron microscopy. To obtain micrographs with transmission electron microscopy (TEM), the JEOL JEM-2100 equipment was used, with a LaB 6 electron gun and an accelerating voltage of 200 kV, operating in TEM mode, with spatial resolutions of 0.25 nm and 1 nm, respectively. Meanwhile, to obtain micrographs with the scanning electron microscope (SEM), the samples were placed on metal stubs, with carbon adhesive tape, and covered with gold. The Quanta FEG 650 field emission gun equipment was used, which had an image detector using secondary electrons (SE). Additionally, energy dispersive spectroscopy (EDS) analysis was performed using the EDAX Apollo X detector, resolution of 126.1 eV (in Mn Kα), using the EDX Genesis software. This analysis allowed obtaining semi-quantitative information on the chemical elements present in the synthesized solids.

To obtain information about the surface of the synthesized ZnO-NPs, X-ray photoelectron spectroscopy (XPS) was used. For this, the Specs NAP-XPS spectrometer was used with a PHOIBOS 150 1D-DLD analyzer and a monochromatic Al-Kα source (1486.7 eV, 13 kV, 100 W), with a pass energy of 86.36 eV for the general spectra and 20 eV for the high resolution spectra. In addition, a step of 1 eV was used for the general spectra, and 0.1 eV for the high resolution spectra. For each high resolution spectrum, 20 cycles were carried out and for the general spectra, five cycles.

Evaluation of the toxicity of synthesized ZnO in Mus musculus biomodels

Ethics

The use and care of the animals in experimentation was carried out considering the laws established by the Colombian Government: (1) Resolution 008430 of October 4, 1993, which establishes the scientific, technical, and administrative standards for health research; Title V, Articles 87 to 93. (2) Law 84 of December 27, 1989; National Statute for the Protection of Animals. (3) Law 576 of 2000, by which the code of ethics for the professional practice of veterinary medicine and zootechnics was established" [55–57]. The present study was endorsed by the Ethics Committee for Scientific Research of the University of Cauca as stated in the record No. 6.1 - 1.25/008 of May 9, 2018.

Determination of the concentrations of ZnO-NPs to form the suspensions to be used in the treatments

To define the concentrations of the synthesized ZnO to be used in the toxicity tests and to obtain representative results from them, a preliminary test was carried out. Based on information reported in the bibliography, on the average exposure limits of ZnO in the air [58, 59], a dose of 100 mg/m^3 was selected, in saline solution (NaCl 0.9 % soln). This suspension was applied to six biomodels, which were exposed to it using a whole-body nebulization chamber (see Fig. 2), for 30 min and two times a day, for a period of one week. This assay allowed us to analyze the behavior of the biomodels and demonstrate histological changes in the NRE. The concentration of 100 mg/m^3 caused significant changes in the behavior of the biomodels, which generated stress in them, for which three doses were established, at concentrations of 6, 15, and 40 mg/m^3, to expose the *Mus musculus* and determine the toxic effect of the ZnO synthesized on them.

The suspensions with the defined concentrations, for the synthesized ZnO, were formed using saline solution as solvent (NaCl 0.9% soln). For this, a solution with a concentration of 100 mg/m^3 was prepared

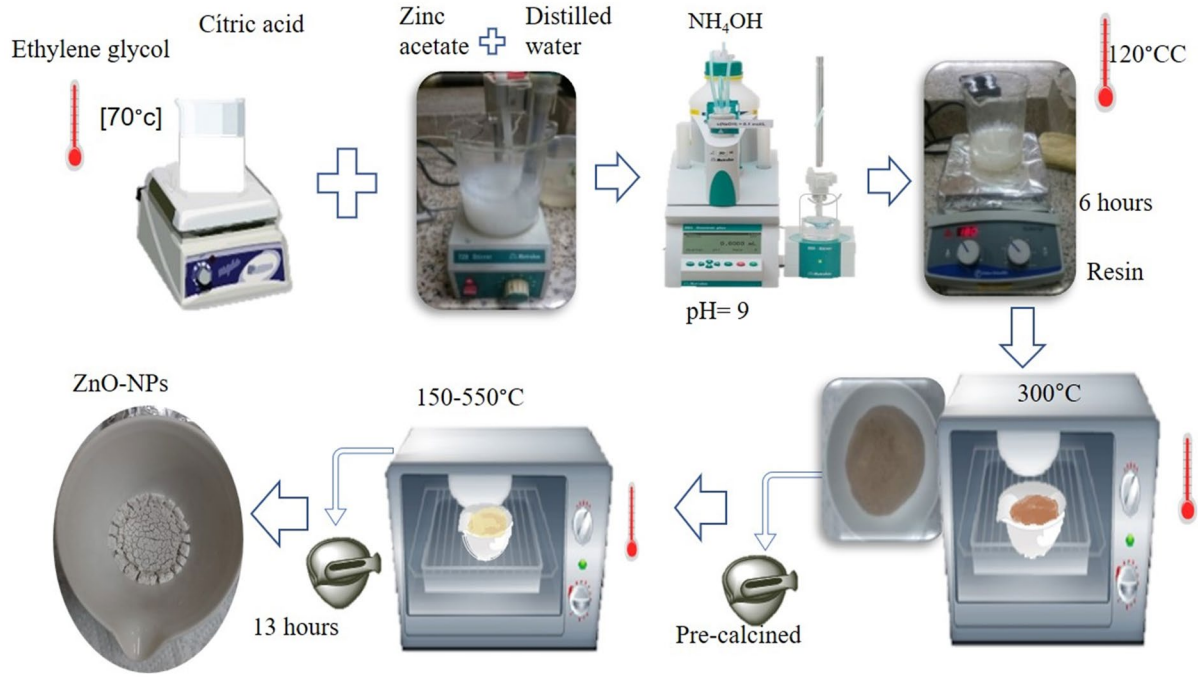

Fig. 1 Diagram of the chemical process used in this work to synthesize the ZnO of interest

and, from this, the high concentration (40 mg/m^3) was obtained, from which it was started to prepare the medium concentration (15 mg/m^3) and, finally, the drop (6 mg/m^3).

Exposure of Mus musculus biomodels to the action of synthesized ZnO

To carry out the tests, 6-week-old male mice of the species *M. musculus* (CFW) were used, obtained at the Intermediate Laboratory for Preclinical Research and Murine Animal Husbandry - Animal Husbandry of the Health Faculty of the Universidad del Valle, in Cali, Colombia), which were adapted to the environment for 2 weeks, before starting the experimentation. When the biomodels reached sexual maturity (8 weeks old), they were divided into four groups (five biomodels per group) and exposed to negative control (0.9% saline solution), low dose (6 mg/m^3), medium dose (15 mg/m^3), and high dose (40 mg/m^3), considering the concentration of the ZnO suspension to be used [58, 59].

The biomodels were exposed to the action of zinc oxide particles using a full-body inhalation chamber (made by physical engineering students from the Universidad del Cauca in Popayán, Colombia - Fig. 2), for 30 min/day, 3 days/week and in a period of 2 months. Considering the indicated exposure time and taking into account that the life expectancy of *M. musculus* is ~2 years, the test can be considered as chronic. Additionally, the body weight of the biomodels was recorded at baseline, mid-exposure, and before euthanasia [48, 50].

Sampling of the nasal respiratory epithelium (NRE)

Because the nasal cavity of the biomodel is small, it was not possible to biopsy it with a cytological brush and it was necessary to euthanize the individuals. For this, a method that caused the least stress to the biomodels was selected. The intramuscular euthanasia procedure of analgesics and sedatives was chosen: ketamine (100 mg/kg) and xylazine (20 mg/kg), and their subsequent exsanguination with the purpose of eliminating or minimizing pain and stress prior to and during the procedure [60, 61].

To obtain and process the NRE of the *M. musculus* mouse, the protocol proposed by Young (1981) was used, with some modifications. Once

Fig. 2 Biomodels exposed to negative control (0.9% saline solution), using a whole-body inhalation chamber

the corresponding lavage of the nasal cavity was carried out, through the posterior opening of the pharyngeal canal (Fig. 3(a)), we immediately proceeded to place the head in neutral formalin plugged at 10% and allowed to set for 6–72 h. Once the fixation time had elapsed, it was decalcified [62]. This was submerged in a mixture of 15 mL of the decalcifier TBD 1- Hydrochloric acid with 5 mL of distilled water, for a period of 6 h. Subsequently, the tissues were washed twice with 70% alcohol (each for 10 min) and then returned to 20 mL of 4% formaldehyde until the sections were made for histological processing.

The decalcified head was removed from the formalin and placed on a cutting board so that the roof of the mouth (the hard palate) was facing up (Fig. 3(b)). Next, with a scalpel, two cuts were made perpendicular to the plane of the hard palate and the nasal septum: the first cut was anterior to the first palatal crest and the second cut 2–3 mm anterior to the first cut (Fig. 3(b)). A section to be processed was obtained, corresponding to the anterior part of the nasal cavity, which was labeled as Level T1.

In Fig. 4**,** we can see cuts made to the nasal cavity of the biomodels and that were arranged in histological plates to define the most suitable ones to carry out the corresponding analysis. The objective was to obtain representative samples of the nasal respiratory epithelium (NRE) that would allow obtaining adequate and pertinent information on the effect of the ZnO-NPs inhaled by the biomodels. For this, the information on histology of the mouse nasal cavity indicated in the book by Ruberte et al. was used as a reference [63].

Subsequently, the selected slides were observed with an optical microscope (Fig. 5), and the different types of cells that make up the nasal respiratory epithelium (Figs 5(a) to 5(d)), as well as the lamina propria, were identified. They play an important role in defending against foreign pathogens trying to enter the body [52].

Histological processing of the NRE of Mus musculus and analysis of the corresponding histological slides

The processing and staining of the NRE samples, intended for histological analysis, was carried out using the protocol established by Luna [64] and other authors such as Salazar and Moreno [65] with some modifications made by the technician from the University of Cauca, Albeiro Polanco Osorio. These procedures were developed in the morphology laboratory of the Universidad del Cauca. The modifications that were made considered the concentration of the reagents, the exposure time, and the amount used of them [64, 65]. The histological slides obtained were read by a specialist physician, member of the working group, considering the alterations experienced by the NRE samples after exposure to ZnO-NPs. The histological slides were observed with an optical microscope (Nikon eclipse 80i). Analysis was performed by evaluating squamous metaplasia, vascular congestion, and immune cells in the NRE of the biomodels [52, 66, 67].

Statistical analysis of the data

For the statistical analysis, contingency tables were made based on the frequency of the pathologies found (squamous metaplasia, vascular congestion and immune cells) and the level of severity (not present, abundant, moderate and scarce), in other cases, presence and absence of pathology. In accordance with the nature of the data, the G test was applied to compare the treatments with the control group and it was accepted that there was an association between the variables studied when the p value was less than 0.05. The BioEstat Version 5.3 program was used [68].

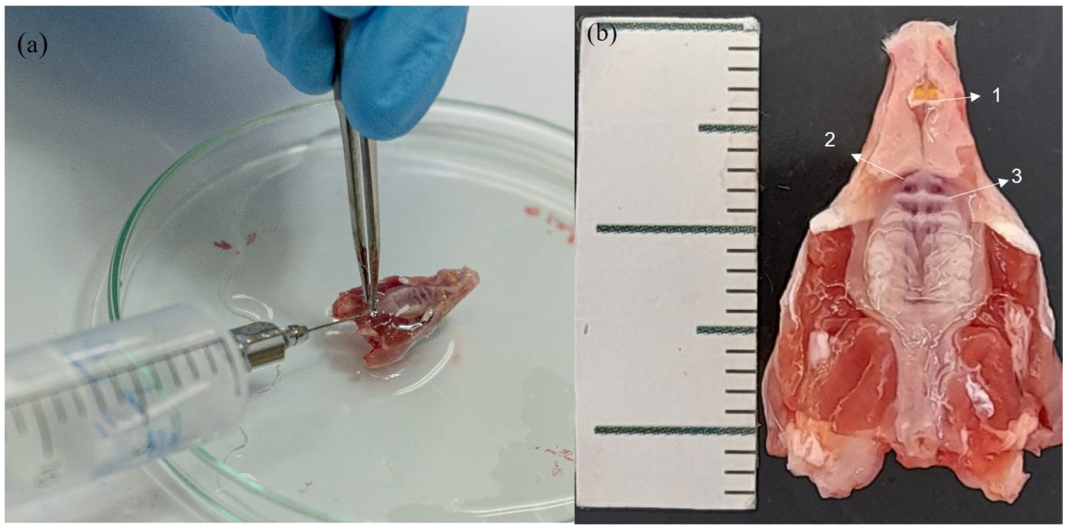

Fig. 3 **a** Washing of the nasal cavity of the *Mus musculus* through the nasopharyngeal canal and **b** hard palate of the head of the biomodels and identification of the areas of interest: (1) upper incisor teeth, (2) incisive papilla, and (3) first palatal crest

Results and discussion

Characterization of the synthesized ZnO particles

Fig. 6(a) shows the IR spectrum corresponding to the ZnO powder synthesized using the Pechini method (Fig. 1) and treated at 550 ºC. The spectrum has a band at ~3440 cm^{-1}, which can be associated with hydroxyl (OH) groups, as well as an intense band located at 450 cm^{-1} that is characteristic of ZnO. In addition, the band at ~1637 cm^{-1} can be associated with water adsorbed by the sample and the small bands located between 1000 and 1600 cm^{-1} and around 2900 cm^{-1} could correspond to carbonaceous groups and C-H groups, respectively, which would be on the surface of the solid.

The Raman spectrum corresponding to ZnO, obtained in this work, is shown in Fig. 6(b). As is known, for a perfect ZnO crystal, only the optical phonons of the point group Γ of the Brillouin zone would be involved in first-order Raman scattering. The optical phonons in the center of the zone predict

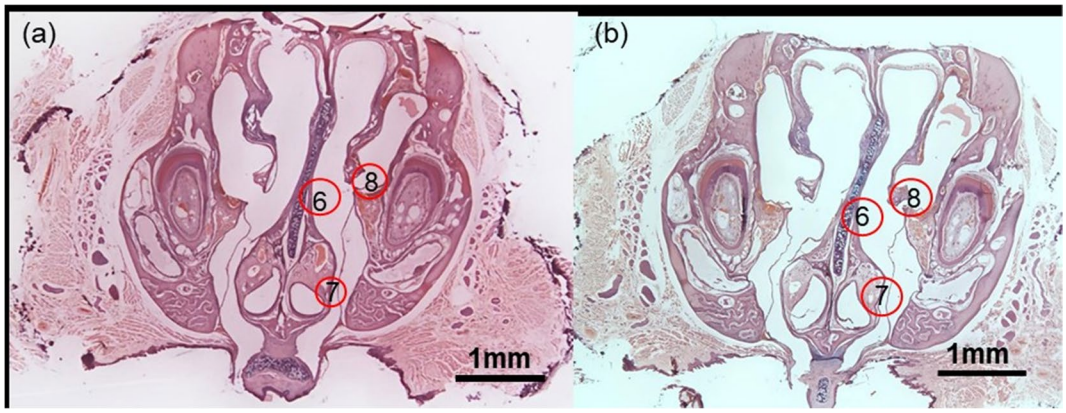

Fig. 4 Observation in the stereoscope of the cross section, at the T1 level, of the biomodels exposed to **a** 0 mg/m^3 and **b** 40 mg/$m.^3$ of ZnO-NPs. [6, respiratory ciliated columnar epithelium; 7, respiratory epithelium with abundant goblet cells; and 8, transient respiratory epithelium]

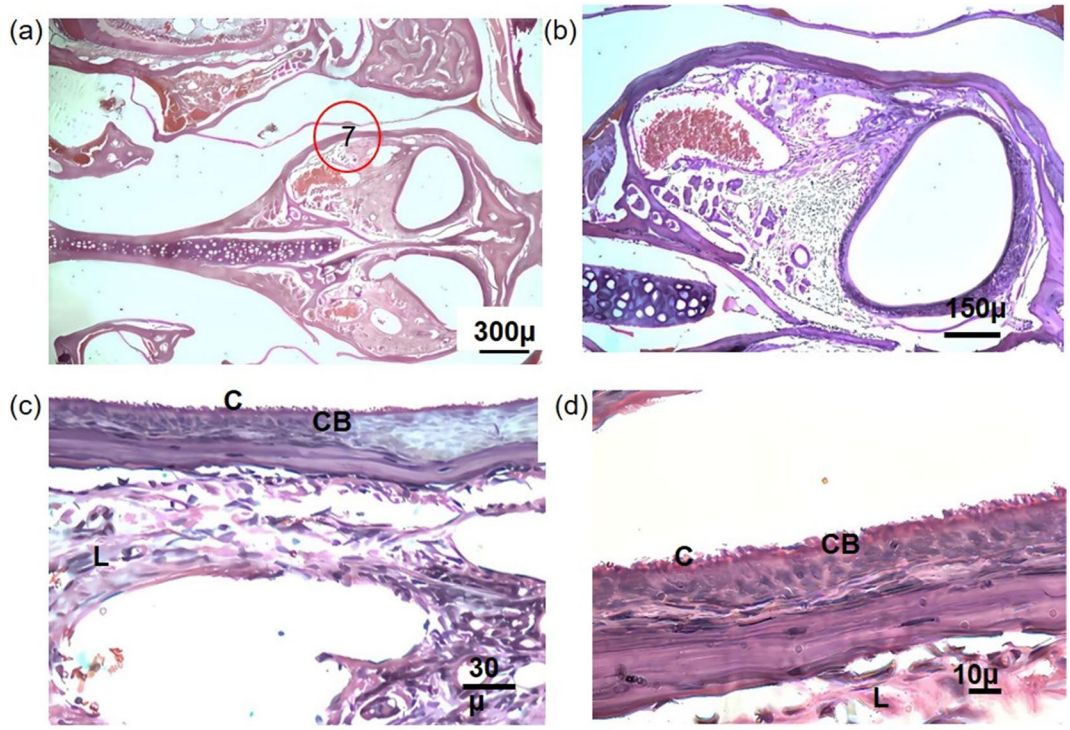

Fig. 5 Micrographs of the magnification of circle 7, of **a** corresponding to the respiratory epithelium, in magnifications of **a** 4X, **b** 10X, **c** 40X, and **d** 100X. [C, columnar hair cells; CB, basal cells; L, Lamina propria. Hematoxylin–eosin staining]

the existence of the following polar modes Γopt = A1 + 2B1 + E1 + 2E2 [69, 70]. Specifically, for the E2 mode, there would be two modes: $E2^{high}$, associated with the vibrations of the oxygen atoms, and $E2^{low}$ associated with the sublattice of Zn atoms.

Despite the high signal-to-noise ratio of the spectrum and the fluorescence spectrum on which the Raman spectrum was supported (Fig. 6(b)), using the information reported in the literature, it was possible to identify the characteristic bands of the ZnO. Those corresponding to the non-resonant $E2^{high}$ mode stand out (see Fig. 6(b)), at ~441 cm^{-1}, mainly associated with the vibration of oxygen and whose pronounced asymmetry can be attributed to the reticular disorder present in the solid (presence of oxygen vacancies), as well as the phenomenon of phononic confinement [71]. In addition, in the spectrum (Fig. 6(b)), the transverse optical modes A1(TO) can be observed, at ~367 cm^{-1}, as well as the linear optical modes A1(LO) at ~573 cm^{-1} that, due to its broadening, would indicate the existence of defects in the crystalline structure of the synthesized oxide. The band observed at ~240 cm^{-1}, exhibits A1 symmetry, and could be attributed to a TA overtone (transverse acoustic mode). For their part, Serrano et al. [70] assigned this band to the 2TA mode, while Calleja et al. [68] attributed it to the $2E2^{low}$ mode. Additionally, in the Raman spectrum of Fig. 6(b), the so-called multiphononic modes and the second-order Raman modes appear, which are mainly located above 600 cm^{-1}. The band at ~640 cm^{-1} would correspond to TA+LO combinations, while the one located at ~699 cm^{-1} could be attributed to combinations of the LA + TO type [70].

In Fig. 6(c), the X-ray diffractogram of the synthesized ZnO is shown. The solid had a crystalline structure, corresponding to wurtzite-type ZnO (PDF 96-230-0113), well crystallized, as indicated by the slender peaks observed in the diffractogram (Fig. 6(b)). With the XRD data obtained, the crystallite size of the material was determined. For this, the location and width at the mean height of the highest intensity peak were used, which corresponds to the Miller indices (101), data that were entered into the

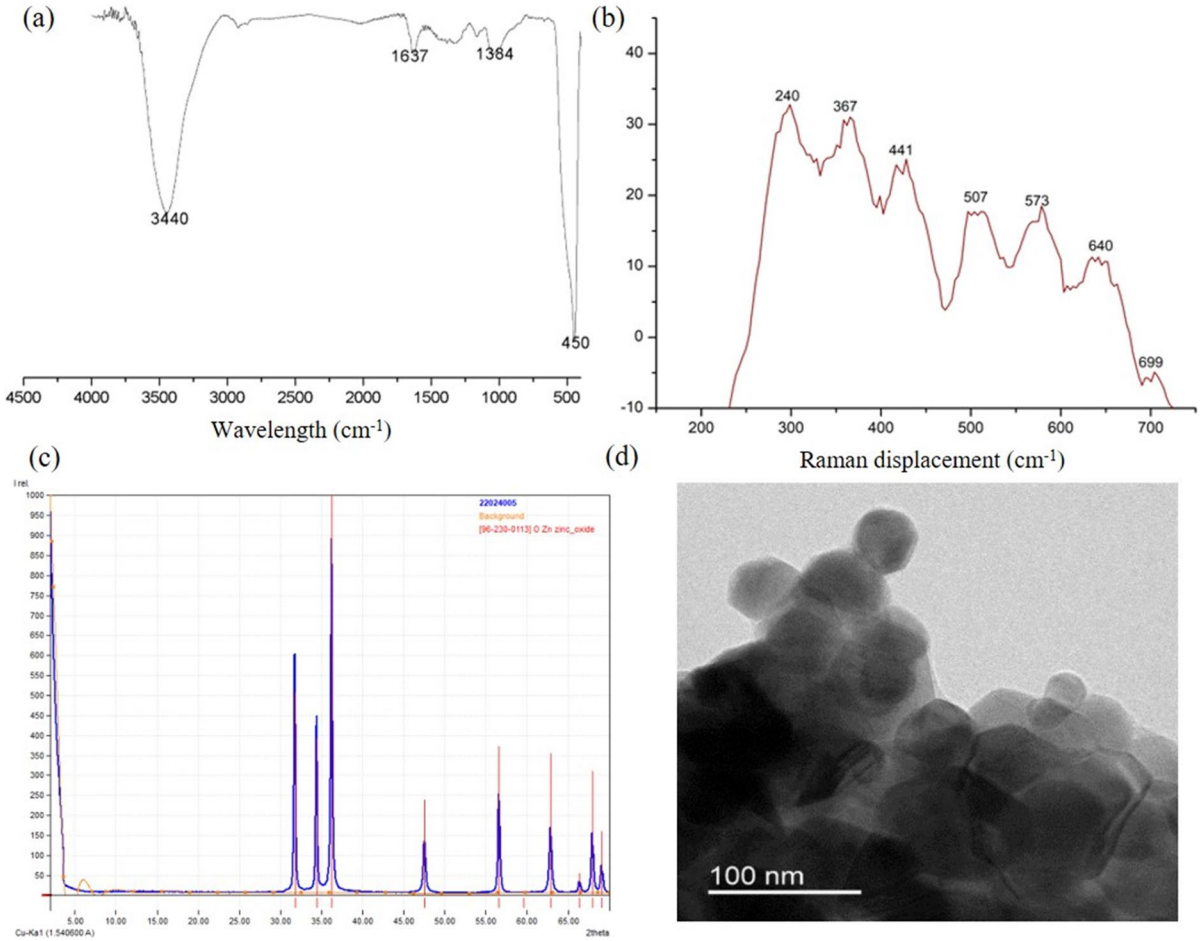

Fig. 6 IR (**a**) and Raman (**b**) spectra, as well as the X-ray diffractogram (**c**) and the TEM microphotograph (**d**) of the ZnO particles synthesized in this work

Debye Scherrer equation $t_c=K\lambda/(\beta Cos(\theta))$, with values of shape factor k=0.9, β=334.8 and λ=1.54060 Å. Calculation of this parameter indicated that the crystallite size of the synthesized ZnO had a value of ~ 41 nm.

In the micrograph obtained with TEM (Fig. 6(d)), it can be seen that the primary ZnO particles had a spheroidal morphology, with a particle size of ~ 50 nm and a tendency to form agglomerates. Comparing the values obtained for crystallite size (~ 41 nm) and mean particle size (~ 50 nm), it can be concluded that the primary particles were monocrystalline.

In the micrographs obtained using SEM (Figs. 7(a) and 7(b)), large agglomerates of the order of microns are observed, as well as small agglomerates with a size of ~ 500 nm. In addition, what was observed with TEM (Fig. 6d) is reiterated, that the primary particles had a size of less than 100 nm (inset Fig. 7(b)). Additionally, EDS spectroscopy was used to determine the elemental chemical composition of the solid, obtaining the spectrum and the table shown in Fig. 7(c). The spectrum indicates that the elements present in the sample were Zn, O, and C and according to the compositional data, given in the table (Fig. 7(c)), the sample had an adequate stoichiometry (considering that the atomic mass of O is 15.99 u and that of Zn 65.38 u), with the main impurity carbon (12.011 u).

The XPS spectroscopy results corresponding to the synthesized ZnO are indicated in Fig. 8 and its general spectrum is shown in Fig. 8(a). The deconvolved spectrum, corresponding to the Zn 2p signal (Fig. 8(b)), presents peaks at 1023.69 eV and

1046.84 eV that can be assigned to Zn ($2p_{3/2}$) and Zn ($2p_{1/2}$), respectively [72]. Furthermore, the peaks located at 976.37 and 1005.21 eV, according to theoretical calculations carried out by Rössler et al. [73], suggest the presence of "clusters" of ZnO on the surface of the solid. The sharp geometry of the first peak may indicate that the Zn element exists on the sample surface mainly in the form of Zn^{2+}.

Figure 8(c) shows the deconvolution of the O 1 s signal from the XPS spectrum, highlighting the peaks located at peaks at 532.7 and 533.76 eV. Considering the location of the peaks of the O1s signal reported in the literature [74, 75], those obtained in the present work are displaced with respect to the reference ones, as was also presented in the work of Kwoka et al. [76], and could be attributed to chemisorbed oxygen species—Oi or oxygens weakly bound to the surface (for example O_2, H_2O or adsorbed hydroxyl groups), associated with the 532.7 eV peak, and to the O-C = O adventitious carbon dioxide bond on the ZnO surface, corresponding to the peak located at 533.76 eV.

The deconvolved spectrum of the C 1 s signal (Fig. 8(d)) presented a peak located at 287.7 eV that could be associated with the C = O bond, both from the adsorbed CO_2 and structural carbonate species [77]. The peak located at 291.9 eV would correspond to the O-C = O adventitious carbon dioxide bond linked to the ZnO surface and the peaks at 284.03 and 285.64 eV could provide information on the Zn–O-C and Zn-C bonds, respectively [78]. It needs stating that there is no complete agreement in the literature on the assignment of the C 1 s peaks of the XPS spectrum with the possible bonds present in the sample. This situation can be seen, for example, in the assignment made by Pan et al. [79] to the C1s signal that they observed in the ZnO (e.g. -CO_3, C-O and C = O bonds). Furthermore, as indicated by Al-Gaashani et al. In their work [80], the location of the peaks in the XPS spectrum would be affected by the morphology of the ZnO-NPs.

Histological analysis of the NRE

Qualitative histological analysis of the NRE of biomodels that inhaled ZnO-NPs

The histopathological evaluation of the NRE of the *M. musculus* biomodels, after 8 weeks of exposure to atmospheres enriched with the synthesized ZnO-NPs, showed a temporary — reversible action of these on the nasal tissue (Fig. 9). On exposure to 0 mg/m^3 (saline solution), the NRE without atypia composed of abundant hair cells lining the nasal cavity was observed (Fig. 9(a)). However, 40% were found to have polymorphonuclear (PMN) leukocytes in the lumen of the nose and only 20% had degranulating mast cells. On the other hand, exposure of biomodels to chemically synthesized ZnO-NPs induced loss of cilia or squamous metaplasia (Fig. 9(b)) and inflammatory infiltrate composed mainly of inflammatory cells, nuclear polymorphs (PMN) in intranasal clusters (Fig. 9(c)), abundant (100% of the population)—moderate and scarce (80% of the population) for the biomodels exposed to 40 mg/m^3 (Fig. 9(b)), 15 mg/m^3 (Fig. 9(c)) and 6 mg/m^3 (Fig. 9(d)), respectively.

Another alteration that was observed in the samples analyzed was the congestion of the nasal vessels (Figs. 9(b) and (c)). Inhalation of ZnO-NPs induced moderate and scarce vascular congestion for exposures at 40 and 15 mg/m^3, respectively, while for exposure at 6 mg/m^3, this effect was not observed. Also, alterations in the NRE related to mast cell granulation were found to occur. It was also found that exposure to 40 mg/m^3 (Fig. 9(b)) caused granulation of mast cells at different levels (abundant, moderate and scarce), while exposure to 15 mg/m^3 (Fig. 9(c)) and 6 mg/m^3 (Fig. 9(d)) produced abundant and moderate, mainly, and scarce effects, respectively (see Fig. 10). In addition, it was observed that when exposing the biomodels to atmospheres with 6 mg/m^3 of ZnO-NPs, immune cells appeared, such as plasma cells (plasmocytes) and accumulations of lymphocytes, located under the epithelium (see Fig. 9(d)).

After the qualitative histological analysis of the different samples, to estimate the histopathological lesions caused by the inhalation of synthesized ZnO-NPs atmospheres, Fig. 10 shows the histopathological evaluation in categories of abundant, moderate, scarce or not found, of (a) squamous metaplasia, (b) nuclear polymorphs, (c) vascular congestion, and (d) mast cell degranulation. To complement the information indicated in Fig. 9, on the histopathological lesions observed in the NRE of *Mus musculus* that inhaled ZnO-NPs, the categorization of the alterations indicated above was carried out considering the presence or absence of: plasma cells and lymphocytes (Fig. 11).

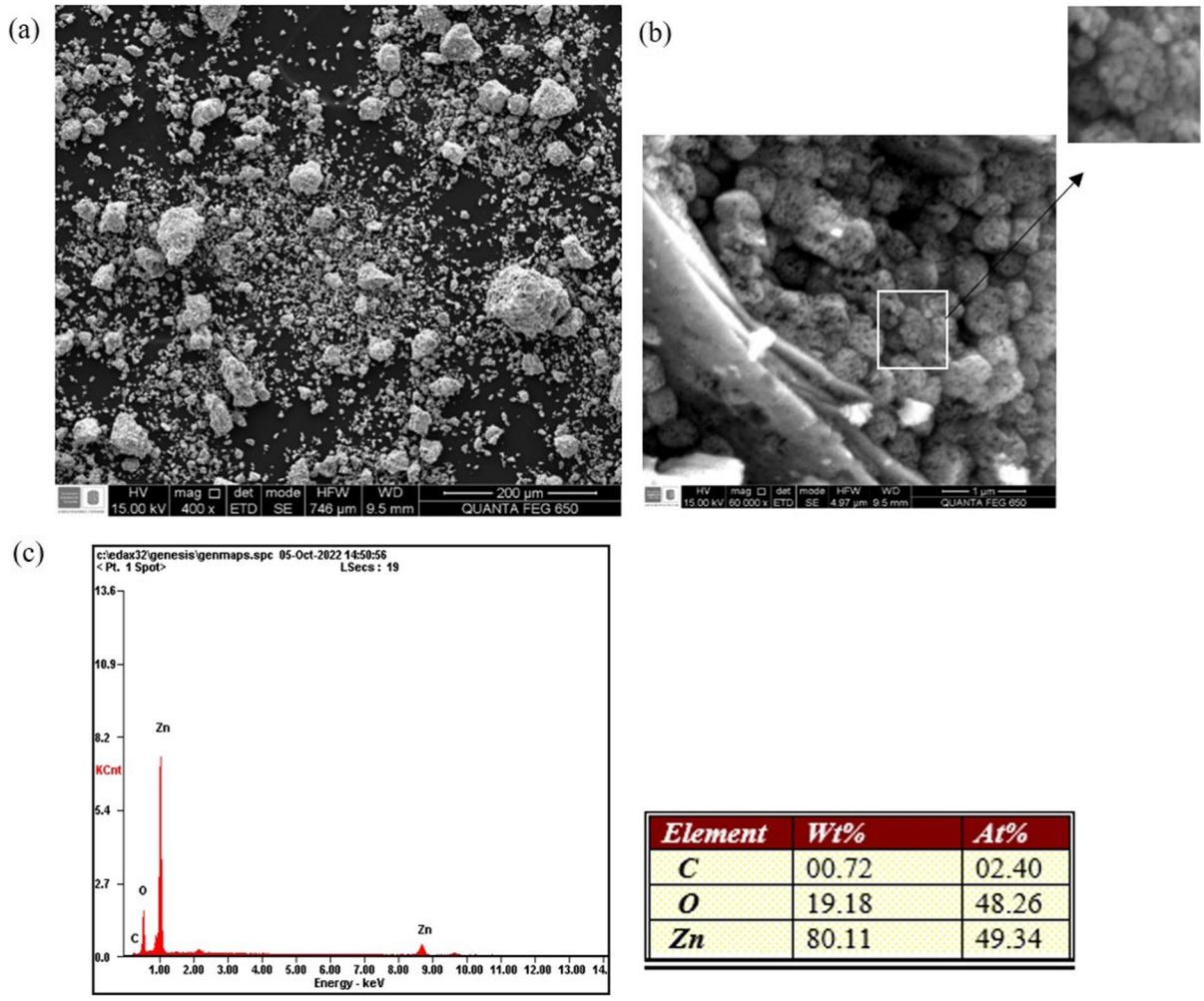

Fig. 7 SEM photographs of the ZnO powders synthesized in this work, **a** by 400X and **b** 60000X, and **c** their corresponding EDX spectrum

Statistical analysis

In this study, it was evidenced that the inhalation of ZnO-NPs induced changes in the NRE of the biomodels. According to the statistical analysis, using the G test, significant differences were observed in PMN alterations, vascular congestion, and squamous metaplasia, with a p value of <0.0001 for the biomodels exposed to the inhalation of ZnO-NPs (see Fig. 10). In this same sense, the presence of immune cells, such as lymphocytes and plasma cells underlying the NRE and in the lamina propria (see Fig. 11), showed a significant difference in the exposure of ZnO-NPs with a p value of 0.0171. However, the presence of degranulating mast cells in the NRE gave, for the G test, a p value of 0.5098 for the exposure of the biomodels to ZnO-NPs. These results indicate that the alteration was not significant.

Discussion of the alterations found in the NRE of the biomodels exposed to ZnO-NPs

Lesions in the NRE of *Mus musculus*, induced by exposure to atmospheres containing the ZnO-NPs obtained in the present study, suggest that inhalation induced inflammatory reactions and morphological changes. Inflammatory reactions would be caused by the immune system, the first line of

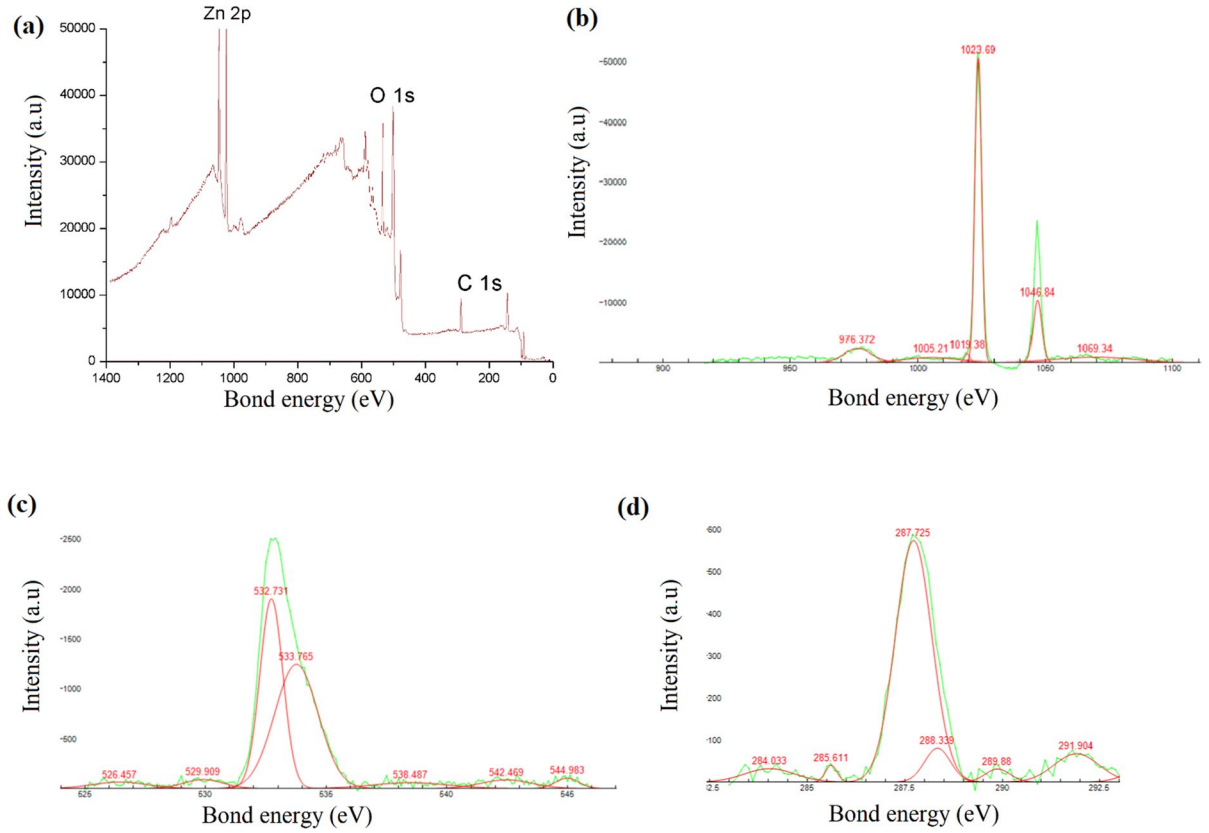

Fig. 8 **a** XPS spectrum corresponding to the ZnO synthesized in this work using a chemical route and the corresponding deconvolutions of the signals: **b** Zn 2p, **c** O 1 s, and **d** C 1 s

defense (innate immunity), with acute inflammation responses, in which conserved molecular patterns are recognized. This response is activated by various molecules, enzymes, and phagocytic cells, such as macrophages and neutrophils, as well as inflammatory cells (mast cells and basophils) [81].

In this stage, inflammatory cells, such as PMN leukocytes (mostly neutrophils, few eosinophils and basophils), migrate from the blood vessels and infiltrate the lamina propria and NRE, to combat potentially harmful substances to which the brain has been exposed. organism [52]. This response would be significantly induced upon exposure of the biomodels to the synthesized ZnO-NPs (Fig. 9(b)). However, it was observed that the induced alteration decreases as the exposure concentration decreases, being abundant for exposure at 40 mg/m^3 and scarce at 6 mg/m^3 (Fig. 10(b)).

It is necessary to remember that innate immunity is very effective. However, it does not protect the body from all infections, so adaptive immunity is activated in weeks, inducing chronic inflammation responses. In this, pathogens to which the organism has never been exposed are recognized, with the leukocytes called T or B lymphocytes coming into play, where the latter differentiate into plasma cells or plasmocytes, producing antibodies that bind to the pathogen to activate the elimination mechanism [82]. Chronic inflammatory responses were evidenced for exposure to 6 mg/m^3 ZnO-NPs (Fig. 9(d)).

Another inflammatory response identified in the NRE was mast cell degranulation. Mast cells are cells resident in the connective tissue (lamina propria) of the nasal mucosa. These have several receptors on their plasma membrane that are activated when the organism comes into contact with pathogens or foreign agents, causing exocytosis of their granules found in their cytoplasm (degranulation) [81, 83]. This initiates and regulates the inflammatory response to eliminate the pathogen agent [82].

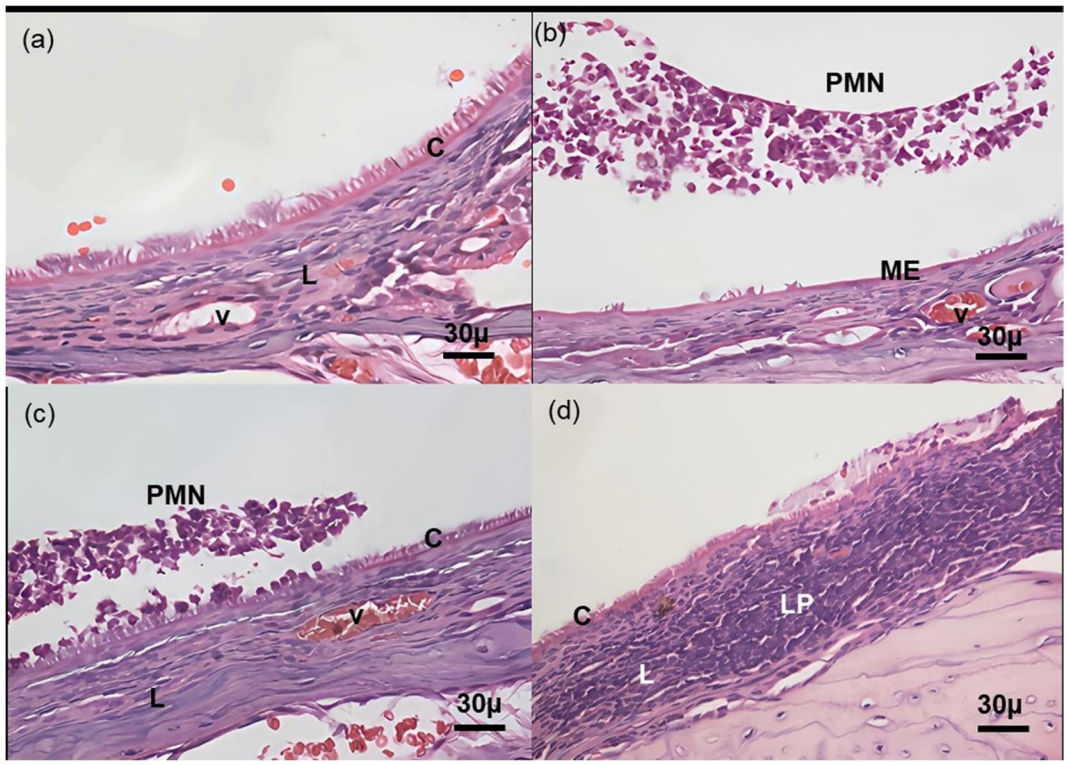

Fig. 9 Qualitative histopathological evaluation and light micrographs of the respiratory nasal epithelium of the biomodels exposed to **a** 0 mg/m^3, **b** 40 mg/m^3, **c** 15 mg/m^3, and **d** 6 mg/m.^{3} of ZnO-NPs synthesized by chemical route (abcd-40X). [C, hair cells; ME, squamous metaplasia; PMN, nuclear polymorphs; V, blood vessels; LP, lymphocytes and plasma cells; L, lamina propria]

Despite the importance of mast cells in inflammatory responses, no significance was found in this study, because this alteration was also identified in the biomodels belonging to the control group (Fig. 10(d)). These results were possibly triggered by employing a whole-body spray chamber (Fig. 2), in which the biomodels caused a drastic change in their microenvironment and, consequently, in the activation of these inflammatory cells.

The morphological changes related to squamous metaplasia (Fig. 9(b)) meanwhile showed high significance in the exposure to ZnO-NPs. Furthermore, it was observed that as the exposure concentration decreased (40, 15, and 6 mg/m^3), the presence of this tissue lesion was scarce (Fig. 10(a)). This histological change contemplates the replacement of the sensitive respiratory epithelium by squamous epithelium that better supports hostile environmental conditions. In this case, it would be more resistant to the injury caused by inhaled NPs. Squamous metaplasia can be identified by the disorganization of the normal respiratory epithelium, with altered polarity of the most superficial cells toward a horizontal orientation with respect to the basal lamina [84].

In this same sense, among the injuries related to exposure to chemical substances or toxic compounds, the complex network of blood vessels of the nasal cavity would be involved [85]. The blood vessels were found to be significantly congested due to the exposure to the ZnO-NPs obtained, being abundant for the exposure of the biomodels at the concentration of 40 mg/m^3 and moderate for that of 15 mg/m^3. Congestion of blood in the blood vessels can change the thickness of the mucosa and cause changes in airflow and nasal resistance [84].

The present research is — at least as far as that which is currently reported in the literature goes — one of the first to describe lesions in the NRE of *M. musculus* biomodels exposed to atmospheres

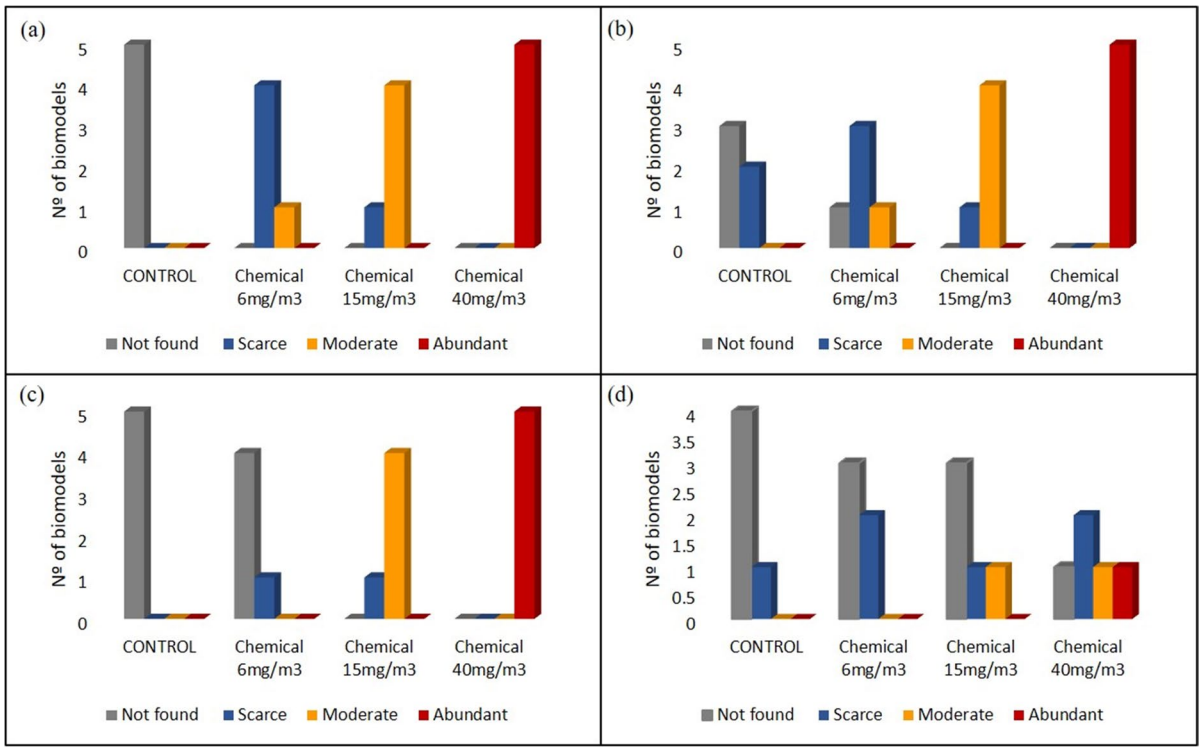

Fig. 10 Bar chart to compare the histopathological lesions caused by the inhalation of ZnO-NPs, with different levels of alterations: abundant, moderate, scarce, and not found, of **a** squamous metaplasia, **b** intranasal nuclear polymorphs, **c** vascular congestion, and **d** degranulating mast cells

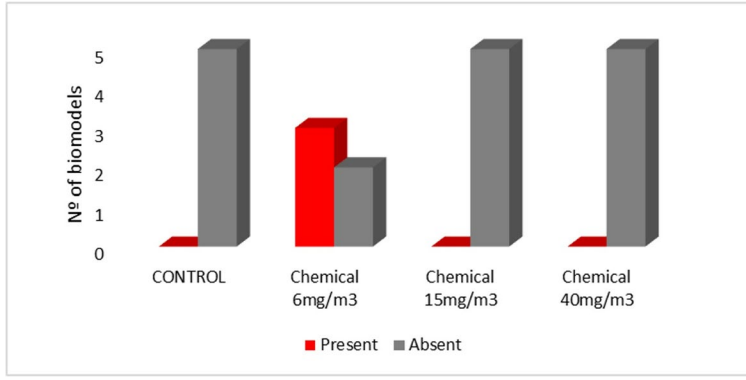

Fig. 11 Bar chart to compare the histopathological lesions caused by the inhalation of synthesized ZnO-NPs, categorizing them as alterations in the presence and/or absence of plasma cells and lymphocytes underlying the epithelium

containing ZnO-NPs synthesized by the Pechini method. Specifically, the histopathologies described in the results of this work, such as squamous metaplasia, vascular congestion, and inflammatory reactions (PMN, mast cells and lymphocytes) in the NRE, are frequent responses in rodents exposed to certain irritating substances or gases, and this is found documented in several studies [66]. For example, repeated exposure to formaldehyde induced alterations in the NRE of the biomodel leading to loss of the mucosal cells and the cilia (squamous metaplasia), hyperplasia or cell proliferation of the mucosal cells, focal neutrophil infiltrates, and vascular congestion [84, 86]. Other substances that, according to the literature, cause changes in hyperplastic, metaplastic and entry and acute

inflammation, with the entry of neutrophils into the lamina propria or the intranasal zone, are ozone [87, 88] chlorine gas [89, 90] and ethylene [91].

In the inhalation studies carried out by other researchers, it is reported that, when the toxic substance is eliminated from the exposure medium in which the biomodel is found, the NRE does not show atypia (squamous metaplasia, hyperplasia, vascular cogestion and/or inflammatory reactions). This occurs after a recovery time of several weeks [66]. Therefore, these are considered reversible histopathologic effects from which NRE frequently suffers. Likewise, these responses of the immune system are an important mechanism, where it is verified that the organism is adequately fighting the external agent.

Although it is not easy to locate specific information on the evaluation of the toxic effect of ZnO-NPs considering the nasal cavity, there are reports of investigations that have evaluated the pulmonary toxicity by inhalation of ZnO-NPs, synthesized by chemical methods, when they pass this first defense of the respiratory system (the NRE) and that would justify the importance of the results obtained in the present work. The results of these investigations indicate that the entry of these nanoparticles, by inhalation, could generate histopathological changes in lung tissue, such as goblet cell hyperplasia, eosinophilic inflammation and fibrosis [92], cell proliferation, PMN leukocytes, foamy macrophages, and lymphocytes [47, 48]. In addition, they highlight that the interaction of ZnO-NPs with lung tissue would occur through endocytosis, where ZnO could dissolve and dissociate into Zn^{2+} [92], causing alteration in Zn homeostasis, producing reactive oxygen species (ROS), form complexes with proteins and probably alter their function [44, 93]. Additionally, these responses are considered in metal fume fever, which causes alteration in proinflammatory cytokines and recruitment of PMN leukocytes, which disappear a few days after exposure to ZnO fume [94].

In the research carried out on the effect of the inhalation of ZnO-NPs, both the exposure time and the concentration of the NPs have been considered. Adamcakova-Dodd et al. [50] showed that inhalation of ZnO-NPs, at a concentration of 3.5 mg/m^3, induced a significant increase in the number of total macrophages and Zn in the lungs, but caused minimal lung inflammation, as well as little cytotoxicity or cell changes. Different results were reported by [47] where the inhalation of ZnO-NP induced foamy lymphocyte and histiocyte infiltration in the alveolar space around the terminal bronchiole, an increase in the neutrophil and eosinophil count in the bronchoalveolar fluid. They therefore concluded that inhalation of ZnO-NPs would induce inflammation in the airways. Moreover, the results obtained in this work disagree with what was reported by [49], this is because exposure to a lower concentration (6 mg/m^3) induced chronic inflammatory responses in the NRE (see Fig, 9**(d)** and Fig. 11), which would be consistent with what was reported by Huang et al. [47], considering that NPs have the ability to travel through the bloodstream and affect other organs, including the lungs.

Other studies, such as the one carried out by Cho et al. [92], considered that ZnO-NPs have the ability to agglomerate and this should influence the toxicity of the system due to the reduction of its specific surface area and therefore its chemical reactivity. They observed that large, randomly dispersed agglomerates could trigger minor inflammatory reactions compared to well-dispersed ZnO-NPs. Therefore, they hypothesize that when ZnO-NPs are well dispersed, the induced inflammatory reactions in the tissue may be of a higher proportion [48]. This hypothesis could account for some of the results found in our research; thus, for example, that the low concentration (6 mg/m^3) of ZnO-NPs was the one that induced chronic inflammatory reactions. This behavior would be more evident for this concentration because the nanoparticles would be more dispersed at the moment of inhalation and their specific surface area would be greater (increasing their reactivity), which would cause a greater adsorption in the NRE. However, a more rigorous study must be carried out to verify this hypothesis.

As indicated by the results reported in the literature on the effects of inhalation of ZnO-NPs on the lung, it is likely that exposure to ZnO-NPs involves the dissolution and dissociation processes of ZnO, such that the Zn^{2+} would promote acute inflammatory reactions with PMN recruitment and morphological changes such as squamous metaplasia and vascular congestion for high exposure concentrations (40 and 15mg/m^3). Moreover, Zn^{2+} could cause chronic inflammatory reactions for the low exposure concentration (6 mg/m^3), with the presence of accumulations of lymphocytes and plasma cells underlying the epithelium.

In general, the issue of air pollution and the presence of particulate matter in it has always been of great interest considering the diseases it might generate [95], specifically lung cancer [96, 97]. Interest in this topic has recently increased due to the uses that can be made of nanoparticles, for example, when their spraying on agricultural crops is required, given their potential as nanofungicides, nanopesticides, and/or nanofertilizers [4, 5, 14]. As mentioned in the introduction, this led to the structuring of a new field of knowledge called nanotoxicity [37] where different mechanisms have been evaluated and researched to account for and explain nanoparticle toxicity. Among the mechanisms discussed are direct nanoparticle association with an organism's cell surface — where the membrane can be damaged or initiate internal signaling pathways that damage the cell, cause disintegration or dissolution of the nanoparticles, leading to the release of toxic ions that impact the organism, generally through impairing important enzyme functions or through direct interaction with the cell's DNA; the formation of protein corona; and the generation of reactive oxygen species (ROS) and subsequent oxidative stress on an organism — which can also damage important enzymes or an organism's genetic material [98, 99]. Studies indicate that the factors that determine the interaction of nanoparticles with biological systems and biomolecules, specifically their toxicity, are their physicochemical properties, such as nanoparticle composition, size, surface chemistry, shape and state of agglomeration [100–102]. Because these properties are heterogeneous in the synthesized nanoparticles, it is not easy to evaluate and understand their interaction with biological systems, adverse effects, and toxicity. In the specific case of ZnO-NPs, the nanomaterial considered in the present work, it is reported that the generation of ROS (which can be either protective or harmful during biological interactions) and therefore oxidative stress, is an important mechanism to explain their toxicity [103]. Furthermore, generation of these ROS can be mediated by the reticular defects of the nanoparticles [38, 104, 105]. The surface chemistry of ZnO-NPs is thus a critical factor in determining the cellular interactions of these nanoparticles with biological systems [106]. Considering the results obtained from the characterization of the ZnO-NPs used in the present work, in addition to the micrographs (Figs. 6(d) and 7) that show their nanometric size and state of agglomeration, the information from the Raman spectroscopy (Fig 6(b)) and XPS (Fig. 8) would indicate the presence of structural defects and for this reason, it could be reiterated that one of the most important toxicity mechanisms in the present toxicity evaluation of ZnO-NPs on the respiratory nasal epithelium would be the generation of ROS, a proposal that ought to be evaluated more systematically, in greater detail, in future research work.

In order to reach a greater understanding of the toxicity of nanoparticles, in general, and of ZnO-NPs in particular, it is therefore necessary to put forward perspectives with new approaches. We hope that the results obtained in this work are a contribution of interest to research on toxicity due to inhalation of nanoparticles and that they also motivate future work to expand our understanding of the toxicity of nanoparticles, in general.

Conclusions

The synthesis methodology used made it possible to obtain ZnO-NPs in a controlled, reproducible way. The characterization techniques used showed that ZnO-NPs smaller than 100 nm in size were obtained, with spheroidal morphology and a tendency to form agglomerates. Additionally, on carrying out the tests that allowed evaluating the lesions in the NRE of the biomodels induced by their exposure to atmospheres containing these nanoparticles, they showed that inhalation induced inflammatory reactions and reversible morphological changes. Specifically, for the treatments at high concentrations of ZnO-NPs (40 and 15 mg/m^3), acute inflammatory reactions occurred, with the recruitment of PMNs in the nasal cavity. Moreover, exposure to a low concentration (6 mg/m^3) caused chronic inflammatory reactions with the recruitment of lymphocytes and plasma cells in the lamina propria of the NRE.

Acknowledgements This work was supported by the MINISTERIO DE CIENCIA TECHNOLOGÍA E INNOVACIÓN—Colombia by financing the project code Number 110380762914 Code – CT 781-2019 COLCIENCIAS. We are grateful to the VRI—ID 5129—UNICAUCA for providing logistic support. We are especially grateful to Colin McLachlan for suggestions relating to the English text.

Author contribution P. A. A-G., M. M. R-V., and J. E. R-P. proposed and supervised the project. K. L. A-C., L. P. M-S, A. M-C, P. A. A-G., M. M. R-V., K. E. M-M, and A. M. C-M. conceived and performed the experiments. K. E. M-M, L. P. M-S, P.A.A-G, and J. E. R-P wrote the paper. All the authors

contributed to the results analyses, discussions, and have approved the final version of the paper.

Funding Open Access funding provided by Colombia Consortium.

Declarations

Conflict of interest The authors declare no competing interests.

References

1. Kulkarni SK (2015) Nanotechnology: principles and practices, 3rd edn. Springer International Publishing, Cham-Switzerland
2. Poole CP Jr, Owens FJ (2003) Introduction to nanotechnology. John Wiley & Sons Inc., Hoboken-New Jersey
3. Valdez FL, Fernández-Luqueño F (2018) Agricultural nanobiotechnology: modern agriculture for a sustainable future. Springer Nature, Switzerland AG. https://doi.org/10.1007/978-3-319-96719-6
4. Fernandez-Luqueno F, Patra KJ (2023) Agricultural and Environmental nanotechnology: novel technologies and their ecological impact. Springer Nature Singapore Pte Ltd., Singapore
5. Panpatte DG, Jhala YK (2019) Nanotechnology for agriculture: crop production & protection. Springer Nature Singapore Pte Ltd., Singapore
6. Jogaiah S, Singh HB, Fernandes-Fraceto L, De Lima R (2021) Advances in nano-fertilizers and nano-pesticides in agriculture. Woodhead Publishing - Elsevier Inc, Cambridge
7. Koul O (2019) Nano-biopesticides today and-future perspectives. Academic Press-Elsevier Inc, San Diego
8. Arciniegas-Grijalba P, Patiño Portela M, Mosquera Sanchez LP, Guerrero Vargas JA, Rodríguez Páez JE (2017) ZnO nanoparticles (ZnO-NPs) and their antifungal activity against coffee fungus Erythricium salmonicolor. Appl Nanosci 7:225–241. https://doi.org/10.1007/s13204-017-0561-3
9. Mosquera Sánchez LP, ArciniegasGrijalba PA, Patiño Portela MC, Guerra Sierra BE, Muñoz Florez JE, Rodríguez Páez JE (2020) Antifungal effect of zinc oxide nanoparticles (ZnO-NPs) on Colletotrichum sp., causal agent of anthracnose in coffee crops. Biocatal Agric Biotechnol 25:101579. https://doi.org/10.1016/j.bcab.2020.101579
10. Patiño-Portela MC, Sánchez-Mosquera LP, Guerra Sierra BE, Muñoz-Florez JE, Eraso-Castillo LA, Rodríguez-Páez JE (2021) Effect of method of synthesis on antifungal ability of ZnO nanoparticles chemical route vs green route. Adv Nano Res 10(2):191–210. https://doi.org/10.12989/anr.2020.10.2.000
11. Lopez-Lima D, Mtz-Enriquez AI, Carrión G, Basurto-Cereceda S, Pariona N (2021) The bifunctional role of copper nanoparticles in tomato: effective treatment for Fusarium wilt and plant growth promoter. Sci Hortic 277:109810. https://doi.org/10.1016/j.scienta.2020.109810
12. Mishra S, Singh BR, Singh A, Keswani C, Naqvi AH, Singh HB (2014) Biofabricated silver nanoparticles act as a strong fungicide against Bipolaris sorokiniana causing spot blotch disease in wheat. PLoS ONE 9(5):e97881. https://doi.org/10.1371/journal.pone.0097881
13. Chávez-Magdaleno ME, González-Estrada RR, Ramos-Guerrero A, Plascencia-Jatomea M, Gutiérrez-Martínez P (2018) Effect of pepper tree (*Schinus molle*) essential oil-loaded chitosan bio-nanocomposites on postharvest control of Colletotrichum gloeosporioides and quality evaluations in avocado (Persea americana) cv. Hass Food Sci Biotechnol 27(6):1871–1875. https://doi.org/10.1007/s10068-018-0410-5
14. Chand MS, Raj S, Trivedi R (2020) Nanotechnology a novel approach to enhance crop productivity. Biochem Biophys Rep 24:100821. https://doi.org/10.1016/j.bbrep.2020.100821
15. Saeedi M, Eslamifar M, Khezri K, Dizaj SM (2019) Applications of nanotechnology in drug delivery to the central nervous system. Biomed Pharmacother 111:666–675. https://doi.org/10.1016/j.biopha.2018.12.133
16. Li C, Zhang H, Gong X, Li Q, Zhao X (2019) Synthesis, characterization, and cytotoxicity assessment of N-acetyl-L-cysteine capped ZnO nanoparticles as camptothecin delivery system. Colloids Surf B Biointerfaces 174:476–482. https://doi.org/10.1016/j.colsurfb.2018.11.043
17. Mishra PK, Mishra H, Ekielski A, Talegaonkar S, Vaidya B (2017) Zinc oxide nanoparticles: a promising nanomaterial for biomedical applications. Drug Discov Today 22(12):1825–1834. https://doi.org/10.1016/j.drudis.2017.08.006
18. Salata OV (2004) Applications of nanoparticles in biology and medicine. Journal of Nanobiotechnology 2:3. https://doi.org/10.1186/1477-3155-2-3
19. Selmaní A, Kovačević D, Bohinc K (2022) Nanoparticles: from synthesis to applications and beyond. Adv Coll Interface Sci 303:102640. https://doi.org/10.1016/j.cis.2022.102640
20. Awasthi K (2021) Nanostructured zinc oxide: synthesis, properties and applications. Elsevier Inc., Amsterdam
21. Klingshirn CF, Meyer BK, Waag A, Hoffmann A, Geurts J (2010) Zin oxide: from fundamental properties towards novel applications. Springer-Verlag, Berlin Heidelberg
22. Bandeira M, Giovanela M, Roesch-Ely M, Devine DM, da Silva CJ (2020) Green synthesis of zinc oxide nanoparticles: a review of the synthesis methodology and mechanism of formation. Sustain Chem Pharm 15:100223. https://doi.org/10.1016/j.scp.2020.100223

23. Morkoc H, Ozgur U (2009) Zinc oxide: fundamentals, materials and device technology. WILEY - VCHVerlag GmbH & Co, KGaA, Wenheim
24 Sun XW, Yang Y (2012) ZnO nanostructures and their applications. Pan Stanford Pub, Singapore
25. Willander M (2014) Zinc oxide nanostructures: advances and applications. Pan Stanford Publishing Pte, Ltd, Singapore
26. Abd-Elsalam KA (2021) Zinc-based nanostructures for environmental and agricultural applications. Elsevier Inc, Amsterdam
27. Droepenu EK, Wee BS, Chin SF, Kok KY, Maligan MF (2022) Zinc oxide nanoparticles synthesis methods and its effect on morphology: a review. Biointerface Res Appl Chem 12(3):4261–4292. https://doi.org/10.33263/BRIAC123.42614292
28. Jamkhande PG, Ghule NW, Bamer AH, Kalaskar MG (2019) Metal nanoparticles synthesis: an overview on methods of preparation, advantages and disadvantages, and applications. J Drug Deliv Sci Technol 53:101174. https://doi.org/10.1016/j.jddst.2019.101174
29. Kakihana M (2009) Synthesis of high-performance ceramics based on polymerizable complex method. J Ceram Soc Jpn 117(8):857–862
30. Kakihana M, Yoshimura M (1999) Synthesis and characteristics of complex multicomponent oxides prepared by polymer complex method. Bull Chem Soc Jpn 72(7):1427–1443. https://doi.org/10.1246/bcsj.72.1427
31. Mazabuel-Collazos A, Rodríguez-Páez JE (2018) Chemical synthesis and characterization of ZnO–TiO_2 semiconductor nanocomposites: tentative mechanism of particle formation. J Inorg Organomet Polym Mater 28(5):1739–1752. https://doi.org/10.1007/s10904-018-0827-6
32. Hussain Z et al (2020) A review of imperative concerns against clinical translation of nanomaterials: unwanted biological interactions of nanomaterials cause serious nanotoxicity. J Drug Deliv Sci Technol 59:101867. https://doi.org/10.1016/j.jddst.2020.101867
33. Nel A, Xia T, Mädler L, Li N (2006) Toxic potential of materials at the nanolevel. Science 311:622–627. https://doi.org/10.1126/science.1114397
34. Oberdörster G (2000) Toxicology of ultrafine particles: in vivo studies. Phil Trans R Soc Lond A 358(1775):2719–2740. https://doi.org/10.1098/rsta.2000.0680
35. Brayner R (2008) The toxicological impact of nanoparticles. Nanotoday 3(1–2):48–55
36. Król A, Pomastowski P, Rafińska K, Railean-Plugaru V, Buszewski B (2017) Zinc oxide nanoparticles: synthesis, antiseptic activity and toxicity mechanism. Adv Colloid Interface Sci 249:37–52. https://doi.org/10.1016/j.cis.2017.07.033
37. Oberdörster G, Oberdörster E, Oberdörster J (2005) Nanotoxicology: an emerging discipline evolving from studies of ultrafine particles. Environ Health Perspect 113(7):823–839. https://doi.org/10.1289/ehp.7339
38. Rodríguez-Páez JE (2021) The semiconductor-cell membrane nano-biointerface: physicochemical phenomena to consider in explaining the nanotoxicity and antifungal capacity of zinc oxide Nanoparticles. Rev Acad Colomb Cienc Ex Fis Nat 45(177):1053–1070. https://doi.org/10.18257/raccefyn.1513
39. Shekhar S, Gautam S, Sharma B, Sharma S, Das PP, Chaudhary V (2021) Deciphering the pathways for evaluation of nanotoxicity: stumbling block in nanotechnology. Clean Eng Technol 5:100311. https://doi.org/10.1016/j.clet.2021.100311
40. Sirelkhatim A et al (2015) Review on zinc oxide nanoparticles: Antibacterial activity and toxicity mechanism. Nanomicro Lett 7(3):219–242. https://doi.org/10.1007/s40820-015-0040-x
41. Moezzi A, McDonagh AM, Cortie MB (2012) Zinc oxide particles: synthesis, properties and applications. Chem Eng J 185–186:1–22. https://doi.org/10.1016/j.cej.2012.01.076
42. Srivastav AK et al (2016) A comprehensive toxicity study of zinc oxide nanoparticles versus their bulk in Wistar rats. Hum Exp Toxicol 35(12):1286–1304. https://doi.org/10.1177/0960327116629530
43. Tang HQ, Xu M, Rong Q, Jin RW, Liu QJ, Li YL (2016) The effect of ZnO nanoparticles on liver function in rats. Int J Nanomedicine 11:4275–4285. https://doi.org/10.2147/IJN.S109031
44. Wang C et al (2016) Effects of long-term exposure to zinc oxide nanoparticles on development, zinc metabolism and biodistribution of minerals (Zn, Fe, Cu, Mn) in mice. PLoS ONE 11(10):e0164434. https://doi.org/10.1371/journal.pone.0164434
45. Huang KL, Lee YH, Chen HI, Liao HS, Chiang BL, Cheng TJ (2015) Zinc oxide nanoparticles induce eosinophilic airway inflammation in mice. J Hazard Mater 297:304–312. https://doi.org/10.1016/j.jhazmat.2015.05.023
46. Luyts K et al (2018) Nanoparticles in the lungs of old mice: pulmonary inflammation and oxidative stress without procoagulant effects. Sci Total Environ 644:907–915. https://doi.org/10.1016/j.scitotenv.2018.06.301
47. Huang KL, Chang HL, Tsai FM, Lee YH, Wang CH, Cheng TJ (2019) The effect of the inhalation of and topical exposure to zinc oxide nanoparticles on airway inflammation in mice. Toxicol Appl Pharmacol 384(17):114787. https://doi.org/10.1016/j.taap.2019.114787
48. Vysloužil J et al (2020) Subchronic continuous inhalation exposure to zinc oxide nanoparticles induces pulmonary cell response in mice. J Trace Elem Med Biol 61:126511. https://doi.org/10.1016/j.jtemb.2020.126511
49. Sruthi S, Ashtami J, Mohanan PV (2018) Biomedical application and hidden toxicity of zinc oxide nanoparticles. Mater Today Chem 10:175–186. https://doi.org/10.1016/j.mtchem.2018.09.008
50. Adamcakova-Dodd A et al (2014) Toxicity assessment of zinc oxide nanoparticles using sub-acute and sub-chronic murine inhalation models. Part Fibre Toxicol 11(15):1–15. https://doi.org/10.1186/1743-8977-11-15
51. Santana Báez S, Mendoza Martín M, Quevedo Villegas MC, Gutiérrez Disla EJ (2018) Revisión Sistemática sobre los efectos tóxicos de las nanopartículas metálicas en la salud de los trabajadores. Med Segur Trab 64(252):295–311

52. Ross MH (2017) Sistema Respiratorio. In: Pawlina W. (Ed) Histologia Texto y Atlas, séptima Edición. Wolters Kluwe, Philadelphia. Capítulo 19.
53. Benitez-Salazar MI, Niño-Castaño VE, Dueñas-Cuellar RA, Caldas-Arias L, Fernández I, Rodríguez-Páez JE (2021) Chemical synthesis versus green synthesis to obtain ZnO powders: evaluation of the antibacterial capacity of the nanoparticles obtained by the chemical method. J Environ Chem Eng 9(6):106544. https://doi.org/10.1016/j.jece.2021.106544
54. Salas G, Rosas N, Galeas S, Guerrero V, Debut A (2016) Síntesis de Nanopartículas de ZnO por el Método de Pechini. Revista Politécnica 38(1):43–47
55. B. Congreso de Colombia, "Ley 84 de 1989 Nivel Nacional." Diario Oficial 39120, Bogotá, pp. 1–16, 1989. [Online]. Available: http://www.alcaldiabogota.gov.co/sisjur/normas/Norma1.jsp?i=8242
56. M. de S. República de Colombia (1993) "RESOLUCIÓN Nº 008430 DE 1993." Bogotá.
57. Vásquez LJ, A. (2007) Pautas básicas para el manejo de animales de experimentación en investigación biomédica. Revista de la Facultad de Ciencias de la Salud 9(4):33–37
58. New Jersey/ Departamento en Salud y Servicios para Personas Mayores (2007) "Hoja informativa sobre sustancias peligrosas - Oxido de Zinc." 1–6.
59. Teck (2018) "Metal Zinc Hojas De Datos De Seguridad," *Teck Resources Limited*. Toronto, pp. 1–7. [Online]. Available: http://www.teck.com/media/Zinc-Metal-Spanish-SDS.pdf
60. AVMA, *AVMA Guidelines for the Euthanasia of Animals: 2020 Edition**, 2020.0.1. American Veterinary Medical Association, 2020.
61 Javeriana U (2021) Procedimiento Operativo Estándar. Eutanasia y Necropsia de Animales de Laboratorio, British Small Animal Veterinary Association
62. Young JT (1981) Histopathologic examination of the rat nasal cavity. Fundam Appl Toxicol 312:309–312
63. Ruberte J, Carretero A, Navarro M (2017) Morphological mouse phenotyping: anatomy, histology and imaging. Academic Press - Elsevier, Amsterdam
64. Luna LG (1968) Manual of histologic staining methods of the Armed Forces Institute of Pathology, 3rd edn. McGraw-Hill, New York
65. Salazar L, Moreno F (2016) Comparación de tres tipos de tinciones histoquímicas en secciones histológicas de paladar y lengua de rata Wistar. Salutem Scientia Spiritus 2(2):12–23
66. Harkema JR, Carey SA, Wagner JG (2006) The nose revisited: a brief review of the comparative structure, function, and toxicologic pathology of the nasal epithelium. Toxicol Pathol 34(3):252–269. https://doi.org/10.1080/01926230600713475
67. Renne RA, Gideon KM, Harbo SJ, Staska LM, Grumbein SL (2007) Upper respiratory tract lesions in inhalation toxicology. Toxicol Pathol 35(1):163–169. https://doi.org/10.1080/01926230601052667
68. A. D. A. SANTOS Dos Santos (2007) *BIOESTAT-aplicações estatísticas nas áreas das Ciências Bio-Médicas*. Brasil: ResearchGate. [Online]. Available: https://www.researchgate.net/publication/263608962
69. Calleja JM, Cardona M (1977) Resonant Raman scattering in ZnO. Phisical review 16(8):3753–3761
70. Serrano J et al (2004) Raman scattering in β-ZnS. Phys Rev B Condens Matter Mater Phys 69(1):014301. https://doi.org/10.1103/PhysRevB.69.014301
71. Šćepanović M, Grujić-Brojčin M, Vojisavljević K, Bernikc S, Srećković T (2010) Raman study of structural disorder in ZnO nanopowders. J Raman Spectrosc 41(9):914–921. https://doi.org/10.1002/jrs.2546
72. Liang YC, Wang CC (2018) Surface crystal feature-dependent photoactivity of ZnO–ZnS composite rods via hydrothermal sulfidation. RSC Adv 8(9):5063–5507
73. Rössler N, Kotsis K, Staemmler V (2006) Ab initio calculations for the Zn 2s and 2p core level binding energies in Zn oxo compounds and ZnO. Phys Chem Chem Phys 8(6):697–706
74. Chen LC, Tu YJ, Wang YS, Kan RS, Huang CM (2008) Characterization and photoreactivity of N-, S-, and C-doped ZnO under UV and visible light illumination. J Photochem Photobiol A Chem 199:170–178
75. Chen M, Wang Z, Han D, Gu F, Guo G (2011) High-sensitivity NO_2 gas sensors based on flower-like and tube-like ZnO nanomaterials. Sens Actuators, B 157:565–574
76. Kwoka M, Kulis-Kapuscinska A, Zappa D, Comini E, Szuber J (2020) Novel insight on the local surface properties of ZnO nanowires. Nanotechnology 31:465705
77. Mar LG, Timbrell PY, Lamb RN (1993) An XPS study of zinc oxide thin film growth on copper using zinc acetate as a precursor. Thin Solid Films 223(2):341–347
78. Alshammari AS, Chi L, Chen X, Bagabas A, Kramer D, Alromaeh A, Jiang Z (2015) Visible-light photocatalysis on C-doped ZnO derived from polymer-assisted pyrolysis. RSC Adv 5:27690–27698
79. Pan L, Muhammad T, Ma L, Huang ZF, Wang S, Wang L, Zou JJ, Zhang X (2016) MOF-derived C-doped ZnO prepared via a two-step calcination forefficient photocatalysis. Appl Catal B 189:181–191
80 Al-Gaashani R, Radiman S, Daud AR, Tabet N, Al-Douri Y (2013) XPS and optical studies of different morphologies of ZnO nanostructures prepared by microwave methods. Ceramics Int 39:2283–2292
81 Abbas AK, Lichtman AH, Pillai S (2012) Inmunología celular y molecular. Septima Edicion, Elsevier España, Barcelona
82 Ariznavarreta C et al (2005) Fisiología humana. Tercera Edición, Mc Graw Hill, Madrid
83. Reguerio Gonzales JR, Lopez Larrea C, Gonzáles Rodríguez S, Martinez NE (2006) Inmunología Biología y Patología del Sistema Inmune. Editorial Médica Panamericana S. A, Tercera Edicion
84. Monticello TM, Morgan KT, Uraiht L (1990) Nonneoplastic nasal lesions in rats and mice. Environ Health Perspect 85:249–274
85. Treuting P., Dintzis S., Montine K. (2017) Sistema Respitatorio - Cavidades Nasales. In: Broderick T. (Ed.) Comparative Anatomy and Histology a Mouse, Rat, and Human Atlas, Segunda Ed.Chennai: Mica Haley. 85–94. https://doi.org/10.1016/b978-0-12-802900-8.00019-1.
86. Chang JCF, Gross EA, Swenberg JA, Barrow CS (1983) Nasal cavity deposition, histopathology, and cell proliferation after single or repeated formaldehyde exposures in B6C3Fl mice and F-344 rats. Toxicol Appl Pharmacol 68(2):161–176
87. Cho HY, Hotchkiss JA, Harkema JR (1999) Inflammatory and epithelial responses during the development of

ozone-induced mucous cell metaplasia in the nasal epithelium of rats. Toxicol Sci 51(1):135–145
88. Harkema JR, Wagner JG (2019) Innate lymphoid cell–dependent airway epithelial and inflammatory responses to inhaled ozone: a new paradigm in pathogenesis. Toxicol Pathol 47(8):993–1003. https://doi.org/10.1177/0192623319873872
89. Jiang XZ, Buckley LA, Morgan KT (1983) Pathology of toxic responses to the RD50 concentration of chlorine gas in the nasal passages of rats and mice. Toxico Appl Pharmacol 71(2):225–236
90. Wolf DC et al (1995) Two-year inhalation exposure of female and male B5C3F1 mice and F344 rast to chlorine gas induce lesions confined to the nose. Fundam Appl Toxicol 24:111–131
91. Brandenberger C, Hotchkiss JA, Krieger SM, Pottenger LH, Harkema JR (2015) Inhalation exposure to ethylene induces eosinophilic rhinitis and nasal epithelial remodeling in Fischer 344 rats. Chem Biol Interact 241:66–75. https://doi.org/10.1016/j.cbi.2015.09.001
92. Cho WS et al (2011) Progressive severe lung injury by zinc oxide nanoparticles; the role of Zn^{2+} dissolution inside lysosomes. Part Fibre Toxicol 8:27. https://doi.org/10.1186/1743-8977-8-27
93. Kao YY, Chiung YM, Chen YC, Cheng TJ, Liu PS (2012) Zinc oxide nanoparticles interfere with zinc ion homeostasis to cause cytotoxicity. Toxicol Sci 125(2):462–472. https://doi.org/10.1093/toxsci/kfr319
94. Wani AL, Parveen N, Ansari MO, Ahmad MdF, Jameel S, Shadab GGHA (2017) Zinc: an element of extensive medical importance. Curr Med Res Pract 7(3):90–98. https://doi.org/10.1016/j.cmrp.2017.02.006
95. Nel A (2005) Air pollution-related illness: effects of particles. Science 308:804–806
96. Schins RPF (2002) Mechanisms of genotoxicity of particles and fibers. Inhalation Toxicol 14:57–78
97. Knaapen AM, Borm PJA, Albrecht C, Schins RPF (2004) Inhaled particles and lung cancer. Part A: Mechanisms Int J Cancer 109:799–809
98. Yang W, Wang L, Mettenbrink EM, De Angelis PL, Wilhelm S (2021) Nanoparticle toxicology. Annu Rev Pharmacol Toxicol 61:269–289
99. Buchman JT, Hudson-Smith NV, Landy KM, Haynes CL (2019) Understanding nanoparticle toxicity mechanisms to inform redesign strategies to reduce environmental impact. Acc Chem Res 52:1632–1642
100. Awashra M, Młynarz P (2023) The toxicity of nanoparticles and their interaction with cells: an *in vitro* metabolomic perspective. Nanoscale Adv 5:2674–2723
101. Albanese A, Tang PS, Chan WCW (2012) The effect of nanoparticle size, shape, and surface chemistry on biological systems. Annu Rev Biomed Eng 14:1–16
102. Elsaesser A, Howard CV (2012) Toxicology of nanoparticles. Adv Drug Deliv Rev 64:129–137
103 Manke A, Wang L, Rojanasakul Y (2013) Mechanisms of nanoparticle-induced oxidative stress and toxicity. BioMed Res Int 2013:1–15
104. Verma SK, Jha E, Panda PK, Das JK, Thirumurugan A, Suar M, Parashar SKS (2018) Molecular aspects of core-shell intrinsic defect induced enhanced antibacterial activity of ZnO nanocrystals. Nanomedicine 13(1):43–68
105. Prasanna VL, Vijayaraghavan R (2015) Insight into the mechanism of antibacterial activity of ZnO – surface defects mediated reactive oxygen species even in dark. Langmuir 31(33):9155–9162
106. Cypriyana PJJ, Saigeetha S, Angalene JLA, Samrot AV, Kumar SS, Ponniah P, Chakravarthi S (2021) Overview on toxicity of nanoparticles, it's mechanism, models used in toxicity studies and disposal methods – a review. Biocatal Agric Biotechnol 36:102117